

Link inference of noisy delay-coupled networks: Machine learning and opto-electronic experimental tests

2021-12-05

Amitava Banerjee^{†1,2}, Joseph D. Hart^{*3}, Rajarshi Roy^{1,2,4}, Edward Ott^{1,2,5}

1. Department of Physics, University of Maryland, College Park, Maryland 20742, U.S.A.
2. Institute for Research in Electronics and Applied Physics, University of Maryland, College Park, Maryland 20742, U.S.A.
3. Optical Sciences Division, US Naval Research Laboratory, Washington, DC 20375, U.S.A.
4. Institute for Physical Science and Technology, University of Maryland, College Park, Maryland 20742, U.S.A.
5. Department of Electrical and Computer Engineering, University of Maryland, College Park, Maryland 20742, U.S.A.

[†] Corresponding author to contact for codes, data, and accessible versions of the presented materials, email: amitava8196@gmail.com, amitavab@umd.edu

^{*} Corresponding author to contact for details of the experiments performed, email: joseph.hart@nrl.navy.mil

Abstract

We devise a machine learning technique to solve the general problem of inferring network links that have time-delays. The goal is to do this purely from time-series data of the network nodal states. This task has applications in fields ranging from applied physics and engineering to neuroscience and biology. To achieve this, we first train a type of machine learning system known as reservoir computing to mimic the dynamics of the unknown network. We formulate and test a technique that uses the trained parameters of the reservoir system output layer to deduce an estimate of the unknown network structure. Our technique, by its nature, is non-invasive, but is motivated by the widely-used invasive network inference method whereby the responses to active perturbations applied to the network are observed and employed to infer network links (e.g., knocking down genes to infer gene regulatory networks). We test this technique on experimental and simulated data from delay-coupled opto-electronic oscillator networks. We show that the technique often yields very good results particularly if the system does not exhibit synchrony. We also find that the presence of dynamical noise can strikingly enhance the accuracy and ability of our technique, especially in networks that exhibit synchrony.

Key Points

1. Network link inference from observed time series data is a broad problem with applications in fields ranging from applied physics and engineering to neuroscience and biology. The machine learning-based method we introduce offers a unique new direction with great potential promise in this field. Our new paradigm for network link inference is the following two-step procedure: learning and modeling the dynamics of a complex system with machine learning, then using the trained machine learning system as a proxy for the actual system to deduce the system's network structure.
2. Typical networks often have delay along their links, which can be anticipated to be an important factor influencing how well link inference methods perform. Our paper focuses on this important factor. Furthermore, we introduce a convenient experimental platform for testing link inference techniques in delay-coupled networks.
3. In addition to our work's usefulness in multiple disciplines (see point 1 above), we also note that, although our technique is non-invasive, it is conceptually multi-disciplinary, in that it is inspired by an analogy to widely-used invasive "knock-down" techniques in experimental molecular biology and genetics for biochemical and gene regulatory network inference.

Contents

1	Introduction	6
2	Reservoir Computing Methodology for Network Inference	9
2.1	The General Delay-coupled Network	9
2.2	Time Series Prediction with a Reservoir Computer	11
2.3	Our Network Inference Procedure	14
3	Opto-electronic Oscillator Networks	18
3.1	Description of the experiment	18
3.2	Mathematical Model and Numerical Simulations of the Network	20
4	Results of Link Inference Tests	23
4.1	Performance on Simulated Data	23
4.2	Performance on Experimental Data	26
5	Discussion	27
6	Acknowledgements	29

A	Determination of the time-delay from cross-correlation	29
B	Derivation of the discrete-time equation for simulating the opto-electronic system	31

1 Introduction

Dynamically evolving complex networks are ubiquitous in natural and technological systems [1]. Examples include food webs [2], biochemical [3, 4] and gene interaction [5, 6] networks, neural networks [7], human interaction networks [8], and the internet, to mention a few. Inference of the structure of such networks from observation of their dynamics is a key issue with applications such as determination of the connectivity in nervous systems [9–11], mapping of interactions between genes [12] and proteins in biochemical networks [13], distinguishing relationships between species in ecological networks [14, 15], understanding the causal dependencies between elements of the global climate [16], and charting of the invisible dark web of the internet [17]. In many of these problems, we can only passively observe time series data for the states of the different components of the networks and cannot actively perturb the systems in any way. Network inference for these cases has led to several different computational and statistical approaches, including Granger causality [18, 19], transfer entropy [20], causation entropy [21], event timing analysis [22], Bayesian techniques [12, 15, 23, 24], inversion of response functions [25, 26], random forest methods [27], and feature ranking methods [28], among others. In addition, application of machine learning techniques for network inference have recently begun to be explored [27, 29–32]. Based on the surprising success of machine learning across a wide variety of data-based tasks [33, 34], we regard it as a particularly promising approach to the network inference problem.

In this work, we are interested in the common situation of dynamics that evolves through

interactions mediated by the network links along which information transfer is subject to time delay. We propose and test, both experimentally and computationally, a machine learning methodology to infer these time-delayed network interactions. In doing this, we use only the sampled time series data of the network nodal states. We find that our method is successful in both experimental and computational tests, provided the time series we use contains sufficient information for the networks to be inferred. We emphasize that the task of link inference for networks with time delays along their links has, to our knowledge, so far not been addressed using experimental data.

Our approach is based on the previously shown ability of machine learning for the prediction and analysis of dynamical time series data. In particular, we shall use a specific neural network architecture called Reservoir Computing (RC) [35], which has previously been used to analyze time series data from complex and chaotic systems, for such tasks as forecasting spatiotemporally chaotic evolution [36–39], determination of Lyapunov exponents and replication of chaotic attractors [40], chaotic source separation [41, 42], and inference of networks (without link time-delays) [29]. Reservoir computers have been implemented in a variety of platforms [35, 43, 44], e.g., in photonic [45–47], electronic and opto-electronic [48, 49] systems. In our technique, we first train an RC on the time-series data from a delay coupled network. Next we use the trained RC to build a proxy *in silico* model for the actual network. Finally, we employ this trained network to predict how the effect of assumed applied perturbations would spread through the network, thus enabling us to deduce the network structure. This approach allows us to retain the non-invasive nature of computational tools like the transfer entropy, while also retaining the conceptual

advantage of invasive methods [50–52].

We will test our network inference method on both simulated and experimental time series data from delay-coupled opto-electronic oscillator networks. An opto-electronic oscillator with time-delayed feedback is a dynamical system that can display a wide variety of complex behaviors, including periodic dynamics [53], breathers [54], and broadband chaos [55]. Opto-electronic oscillators have found applications in highly stable microwave generation for frequency references [53], neuromorphic computing [56, 57], chaotic communications [58], and sensing [59]. The nonlinear dynamics of individual [60–62] and coupled opto-electronic oscillators [63–66] are well-understood, making networks of opto-electronic oscillators an excellent test bed for network inference techniques.

We find that our method accurately reconstructs the network from experimentally measured time series data, as long as the coupling is sufficiently strong and the network does not display strong global synchronization. We also find that the presence of dynamical noise may have a significant positive effect on the ability to infer links. Our results provide a clear demonstration that reservoir computing, and possibly other related machine learning methods, can provide accurate network inference for real networks, including situations where complications like noise and time delays in the coupling are present.

This paper is organized as follows. In Sec. 2, we introduce our network inference method for a general delay-coupled network dynamical system. In Sec. 3, we present the opto-electronic oscillator networks that we use for testing our method, along with a brief description of the collective dynamics of these networks in different parameter regimes.

Section 4 presents results of our tests of the effectiveness of our method for both simulated and experimental time series data. Finally, we conclude in Sec. 5 with further discussion, suggested future directions, and possible generalizations of our method.

2 Reservoir Computing Methodology for Network Inference

2.1 The General Delay-coupled Network

In this section, we present the principles of our RC-based network link inference method. We consider a system of D_n nodes, with the interactions among them mediated by a network of time-delayed links. We assume that the state of the i -th node in the network is given by a time dependent vector $\mathbf{X}_i[t]$ of dimension D_s , with $i = 1, 2, 3, \dots, D_n$. We denote the components of this vector by X_i^μ with $\mu = 1, 2, 3, \dots, D_s$. The coupled dynamics of the full system is governed by a general delay differential equation of the form

$$\frac{dX_i^\mu(t)}{dt} = \phi_i^\mu(\mathbf{X}_i(t); \mathbf{X}_1(t - \tau), \mathbf{X}_2(t - \tau), \dots, \mathbf{X}_{D_n}(t - \tau); t). \quad (1)$$

Here ϕ_i^μ is the function governing the dynamics of the μ -th component of the state vector of the i -th node. ϕ_i^μ is a function of X_j^ν if and only if there is a network link (connection) from the ν -th component of the state vector of the j -th node to the μ -th component of the state vector of the i -th node. Note that, for simplicity, in the above equation, we assume that the couplings have only a single time delay τ , which is the time it takes a signal to

propagate from one component of the system to another. In the experiments we shall consider here, the time series data from the above dynamics is sampled at a time interval $\Delta t = \tau/k$ (with k being an integer) and are denoted by $\{\mathbf{X}_i[\Delta t]\}, \{\mathbf{X}_i[2\Delta t]\}, \{\mathbf{X}_i[3\Delta t]\}, \dots$ and so on.

The problem we wish to address can be formalized as follows: *If the observed time series data $\{\mathbf{X}_i[t]\}$ is the only information from the system we have, can we infer the connections of the network assuming that the underlying dynamical equations are of the general form as in Eq. (1)?* We note that we lack any explicit knowledge of the functions $\{\phi_i^\mu\}$. However, we shall henceforth assume that we know the delay $\tau = k\Delta t$, which, as shown in Appendix A, can be inferred from the available time series data. Furthermore, we note that the performance of our method is not strongly dependent on the accuracy with which we infer the delay time k . For example, in our cases where we typically had $k = 34$ (corresponding to a delay time $\tau = 1.4\text{ms}$) in the simulations and experiments, setting the inferred value of k anywhere between 34 and 37 (delay time of 1.4ms and 1.5ms, respectively) gave us essentially the same link inference results. Finally, we note that in a general situation, it might not be feasible to sample all the components of the state vectors. So, henceforth we will assume that we may sample only a subset of the components of each of the nodal state vectors $\{\mathbf{X}_i[t]\}$, which, without loss of generality, we designate as the first $D'_s(\leq D_s)$ components. We now turn to a description of RC machine learning.

2.2 Time Series Prediction with a Reservoir Computer

In this work, our first step is to train an RC to predict the time evolution of the node states one delay time $\tau = k\Delta t$ into the future, following which we will use that training information to extract the network structure of the system. A schematic of our RC implementation ([29, 36]) is shown in Fig. 1. We consider an RC network consisting of a large number of nodes D_r (such that $D_r \gg D_n \times D'_s \equiv D_X$). Each of the nodes has a time dependent scalar state, all of which are collected in a column vector \mathbf{R} of length D_r . These reservoir nodes receive measured inputs of the unknown network system states $\{\mathbf{X}_i[t]\}$. We concatenate the sampled input measurements of the time-dependent node state vectors $\{\mathbf{X}_i[t]\}$ and place them in a single time-dependent column vector $\mathcal{X}[t]$ of length D_X , such that the components of $\mathcal{X}[t]$ are arranged as follows;

$$\mathcal{X}[t] = \left(X_1^1[t], X_1^2[t], \dots, X_1^{D'_s}[t], X_2^1[t], X_2^2[t], \dots, X_2^{D'_s}[t], \dots, X_{D_n}^{D'_s}[t] \right)^T. \quad (2)$$

This vector is fed into the reservoir via a $D_r \times D_X$ input-to-reservoir coupling matrix \mathbf{W}_{in} (Fig. 1). Furthermore, the reservoir nodes are coupled among themselves with a $D_r \times D_r$ adjacency matrix \mathbf{H} . The time evolution of the reservoir node states \mathbf{R} are given by the equation,

$$\mathbf{R}[n\Delta t] = \sigma(\mathbf{H}\mathbf{R}[(n-1)\Delta t] + \mathbf{W}_{\text{in}}\mathcal{X}[n\Delta t]), \quad (3)$$

which maps the reservoir state at time $(n-1)\Delta t$ to the reservoir state at the next time step, $n\Delta t$, where n is a positive integer, and σ is a sigmoidal activation function acting componentwise on its vector argument (which has the same dimension, D_r , as \mathbf{R}).

Keeping in mind the form of Eq. (1), our first step is to predict the future values of the sampled components of $\{\mathbf{X}_i [(n+k)\Delta t]\}$ in the concatenated form $\mathcal{X} [(n+k)\Delta t]$ (Eq. (2)) from their current observed values $\mathcal{X} [n\Delta t]$, using the reservoir state vector $\mathbf{R} [n\Delta t]$. In our case, this is done by using a suitable linear combination of the reservoir node states with a $D_X \times D_r$ reservoir-to-output coupling matrix \mathbf{W}_{out} (Fig. 1) according to the equation,

$$\mathcal{X}^P [(n+k)\Delta t] = \mathbf{W}_{\text{out}}\mathbf{R} [n\Delta t], \quad (4)$$

where the superscript P indicates that the vector is a prediction from the RC, as opposed to being sampled from the actual system. During the training time, we measure the system training time series data $\{\mathcal{X} [t]\}$ from the unknown system of interest for a large number of time steps. We use this data along with Eq. (3) to generate the time series data for the RC nodal states, which we store in $\{\mathbf{R} [n\Delta t]\}$. For the training of the RC, we then find the elements of the matrix \mathbf{W}_{out} by doing a linear regression from these stored reservoir states $\mathbf{R} [n\Delta t]$ to the measured time-advanced system states $\{\mathcal{X} [(n+k)\Delta t]\}$ comprising our observed training data, such that Eq. (4) provides a best mean squared fit of the prediction $\mathcal{X}^P [(n+k)\Delta t]$ to the measured state $\mathcal{X} [(n+k)\Delta t]$. This amounts to the minimization of a cost function \mathcal{C} given by

$$\mathcal{C} = \sum_{\text{Training Steps } n} \|\mathcal{X} [(n+k)\Delta t] - \mathbf{W}_{\text{out}}\mathbf{R} [n\Delta t]\|^2 + \lambda \|\mathbf{W}_{\text{out}}\|^2 \quad (5)$$

where the last term ($\lambda \|\mathbf{W}_{\text{out}}\|^2$) is a “ridge” regularization term [67] used to prevent overfitting to the training data and λ is typically a small number.

To completely specify the training procedure that we use, we now specify the structures

of the different associated matrices. The elements of the input matrix \mathbf{W}_{in} are chosen randomly from a uniform distribution in the interval $[-w, w]$. The reservoir connectivity matrix \mathbf{H} is a sparse random matrix, corresponding to an average in-degree d_{av} of the reservoir nodes. The non-zero elements of \mathbf{H} are chosen randomly from an uniform distribution $[-h, h]$ and h is chosen such that the spectral radius of \mathbf{H} (i.e., the maximum magnitude of the eigenvalues of \mathbf{H}) is equal to some predefined value ρ . The hyperparameters w and d_{av} are chosen using a Nelder-Mead optimization procedure where we minimize \mathcal{C} for a representative training data and the corresponding output matrix \mathbf{W}_{out} found from the training data. We checked that the hyperparameter values obtained for different training time series were consistent with each other, so we used their typical values $w = 1.17$ and $d_{\text{av}} = 2.38$ for tests on simulated data and $w = 1.19$ and $d_{\text{av}} = 2.56$ for tests on experimental data. We typically use values $\lambda = 10^{-4}$ and $\rho = 0.9$ for the other two hyperparameters, 3×10^4 steps (about 880 delay times) for training and the sigmoidal activation function σ is taken to be the hyperbolic tangent function. The reservoirs we used typically had 3000 nodes. After a successful training of the RC with these specifications, Eq. (4) can be seen as an *in silico* model for the dynamics of the actual system. (In certain instances, it may be used for predicting the unobserved future evolution of the system, but we will not require this ability for our network inference purpose. Some explanations of these abilities of trained RCs can be found in Refs. [40, 68–70]).

2.3 Our Network Inference Procedure

We now describe how we use the training results of the previous subsection to obtain the network structure of the unknown system. We first briefly discuss how the form of Eq. (1) allows us to relate the network structure to the spread of small perturbations in the system. Suppose that, at a time point $t = n\Delta t$, we perturb the ν -th component of the state of node j by an infinitesimal amount $\delta X_j^\nu [n\Delta t]$. Differentiating both sides of Eq. (1), we see that this perturbation changes the μ -th component of the state of node i ($i \neq j$) at a later time $(n+k)\Delta t = t + \tau$ via the corresponding change in the time derivative,

$$\delta \left(\left. \frac{dX_i^\mu}{dt} \right|_{t+\tau} \right) = \frac{\partial \phi_i^\mu}{\partial X_j^\nu} \delta X_j^\nu [t] + \mathcal{O} \left((\delta X_j^\nu [t])^2 \right). \quad (6)$$

This equation shows that, to lowest order, the effect of the small perturbation on component ν of the state of node j is propagated to the component μ of the state of node i with a delay of $\tau = k\Delta t$ provided that there is a corresponding network link between them, i.e., if $\partial \phi_i^\mu / \partial X_j^\nu \neq 0$. In particular, propagation of a perturbation from component ν of the state of node j to component μ of the state of node i with a delay of k time steps implies that a directional network link, $(j, \nu) \rightarrow (i, \mu)$, exists between them.

While the above discussion is predicated on application of an active perturbation, we see that the result is essentially determined by the partial derivative $\partial \phi_i^\mu / \partial X_j^\nu$. Thus we wish to determine whether this partial derivative is zero (corresponding to the absence of a link) or not (corresponding to the presence of a link). We attempt to do this by use of the trained RC (which, as we emphasize, was obtained solely from observations, i.e., non-invasively). Indeed, when Eq. (4) is approximately true for a well-trained RC with

$\mathcal{X}^P [(n+k)\Delta t] \approx \mathcal{X} [(n+k)\Delta t]$, we can use that equation to consider the RC-predicted dynamics as a proxy for the dynamics of the actual system. In that case, within this assumed RC proxy model, we can analytically assess the effects of small perturbations, and compare them to Eq. (6). To do so, we first combine Eqs. (3) and (4) for the RC, and use the relation $\mathcal{X}^P [(n+k)\Delta t] = \mathcal{X} [(n+k)\Delta t]$ for the training data to obtain the equation,

$$\mathcal{X} [(n+k)\Delta t] = \mathbf{W}_{\text{out}}\sigma(\mathbf{H}\mathbf{R} [(n-1)\Delta t] + \mathbf{W}_{\text{in}}\mathcal{X} [n\Delta t]), \quad (7)$$

where the time points belong to the training time series. In order to evaluate the effect of a perturbation to one node on another, we desire to eliminate reservoir variables \mathbf{R} from this equation. Naively, this could be done by solving Eq. (4) for $\mathbf{R} [(n-1)\Delta t]$ in terms of $\mathcal{X} [(n+k-1)\Delta t]$. However, the number of components of \mathbf{R} is large compared to the number of components of \mathcal{X} , and so there are many solutions of Eq. (4) for \mathbf{R} . As in our previous work [29], we hypothesize (and subsequently test) that, for our purpose, the Moore-Penrose pseudoinverse [71] (symbolically denoted by $\hat{\mathbf{W}}_{\text{out}}^{-1}$) provides a useful solution of the equation $\mathcal{X} [(n+k)\Delta t] = \mathbf{W}_{\text{out}}\mathbf{R} [(n-1)\Delta t]$ for $\mathbf{R} [(n-1)\Delta t]$. With this, Eq. (7) becomes

$$\mathcal{X} [(n+k)\Delta t] = \mathbf{W}_{\text{out}}\sigma\left(\mathbf{H}\hat{\mathbf{W}}_{\text{out}}^{-1}\mathcal{X} [(n+k-1)\Delta t] + \mathbf{W}_{\text{in}}\mathcal{X} [n\Delta t]\right) \quad (8)$$

yielding a putative dynamical model for the system from which we will now study the effect of small perturbations. Thus, an infinitesimal amount of change in the network node states at time step $n\Delta t$, written as $\delta\mathcal{X} [n\Delta t]$, propagates to a change at time $(n+k)\Delta t$

as described by differentiating Eq. (8),

$$\delta\mathcal{X}[(n+k)\Delta t] = \left(\mathbb{1} - \mathbf{W}_{\text{out}}\hat{\mathbf{H}}[n\Delta t]\hat{\mathbf{W}}_{\text{out}}^{-1}\right)^{-1}\mathbf{W}_{\text{out}}\hat{\mathbf{W}}_{\text{in}}[n\Delta t]\delta\mathcal{X}[n\Delta t] \equiv \mathbf{M}[n\Delta t]\delta\mathcal{X}[n\Delta t], \quad (9)$$

where we have used Eq. (3), assumed that Δt is sufficiently small that $\delta\mathcal{X}[(n+k)\Delta t] \approx \delta\mathcal{X}[(n+k-1)\Delta t]$, and defined the new matrix elements $\hat{H}_{ij}[n\Delta t] = H_{ij}\sigma'(R_i[n\Delta t])$ and $\left(\hat{W}_{\text{in}}\right)_{ij}[n\Delta t] = (W_{\text{in}})_{ij}\sigma'(R_i[n\Delta t])$ where $\sigma'(u) = d\sigma(u)/du$. We now employ this equation in component form in the place of Eq. (6) as a proxy approximating how small perturbations spread across the network. In particular, just like the partial derivative $\partial\phi_i^\mu/\partial X_j^\nu$ determines whether a change at the ν -th component of state of node j results in a change of the μ -th component of the state of node i after k time steps in Eq. (6), $M_{i,j}[n\Delta t]$ determines the same in Eq. (9), when used in conjunction with our definition Eq. (2) for $\mathcal{X}[t]$.

We now describe how we use our determination of \mathbf{M} in Eq. (9) to recover the network structure. For this purpose, we are only interested in determining whether $\partial\phi_i^\mu/\partial X_j^\nu$ is zero (no link $(j, \nu) \rightarrow (i, \mu)$) or not. If we had the exact Jacobian, the absence of link would imply $\partial\phi_i^\mu/\partial X_j^\nu = 0$ exactly. However, in our procedure, there are errors and thus the derivatives are never zero. These errors are due to finite reservoir size, finite training data length, noise in the training data, and the Moore-Penrose inversion which, as we hypothesized, is only useful but not exact. For these reasons, we decide whether the elements of \mathbf{M} are zero or not by assigning each of the elements a positive score. If the score is above a threshold, we assume that there is a link, and if the score is less than a threshold, we assume it to be zero. To form an appropriate score for each of the elements

M_{ij} , we use $\langle |M_{ij}| \rangle_t$ where $\langle \rangle_t$ denotes time-averaging over a sufficiently long time. Here the absolute value of M_{ij} is to be taken so that the positive and negative values do not cancel each other while doing the time averaging.

Once we have defined and calculated the score, choosing the threshold is a well-known problem of binary categorization of a collection of continuous numerical scores. This is a basic problem in statistics and addressed extensively in earlier works with methods such as Receiver Operating Characteristic and Precision-Recall curves, fitting to mixtures of statistical distributions, Bayesian techniques etc. In application, the method for the choice of the threshold in binary classification is situation-dependent. To avoid the details of the statistical methodologies, we adopt a procedure which is simple but sufficient for the purpose of evaluation of our link inference method. We shall henceforth assume that we know the total number of links (denoted by L) in the unknown network and shall designate the elements M_{ij} having the largest L scores as nonzero (i.e., corresponding to inferred network links), while those M_{ij} with scores below the largest L scores will be inferred to not correspond to network links. The performance of this link inference technique will be measured by the corresponding number of falsely inferred links (“false positives”). Since we assume that we know the total number of links, the number of falsely inferred links is also equal to the number of missed linked (“false negatives”). As we will see below, this method can produce excellent results in link inference tasks over a wide range of coupling strengths, network topologies, and noise levels.

3 Opto-electronic Oscillator Networks

3.1 Description of the experiment

In this section, we introduce our opto-electronic network used as a platform to test our network inference procedure. An individual opto-electronic oscillator is a nonlinear, time-delayed feedback loop. Our network consists of four nominally identical opto-electronic oscillators with time-delayed optical coupling between them. The individual and coupled dynamics of opto-electronic oscillators have been studied extensively [55, 61, 62, 64–66, 72, 73].

An illustration of a single networked opto-electronic oscillator is shown in Fig. 2. A fiber-coupled continuous-wave laser emits light of constant intensity. The light passes through an intensity modulator, which serves as the nonlinearity in the feedback loop and can be described by $\cos^2(\pi v/2V_\pi)$ where v is the voltage applied to the modulator. For our modulators $V_\pi = 3.4\text{V}$. The light that passes through the modulator is split by a 1×4 coupler. Three of the coupler outputs serve as coupling signals to other three nodes of the network; the remaining output serves as the feedback. The feedback optical signal is converted to an electrical signal by a photodiode, which is then delayed and filtered by a digital signal processing (DSP) board (Texas Instruments TMS320C6713). When an opto-electronic oscillator is operating independently, this signal is output by the DSP board, amplified, and fed back to drive the modulator. The normalized voltage $x(t) \equiv \pi v(t)/2V_\pi$ applied to the intensity modulator is measured and is our dynamical

variable.

In order to couple the opto-electronic oscillator to the network, the incoming optical signals pass through variable optical attenuators, which control the link strengths, then are combined by a 3x1 fiber optic combiner. This optical signal is converted into a coupling electrical signal by a second photodiode. This coupling electrical signal is combined with the feedback signal in the DSP board such that the coupling is Laplacian. The DSP also delays and filters the combined signal. This combined signal is output by the DSP, amplified, and used to drive the modulator. The ratio of amplification factors of the coupling signal and feedback signal is given by the coupling strength ϵ .

The amplifier gain is set such that each feedback loop has identical round-trip gain β . Each link also has the same time delay $\tau = 1.4$ ms. We choose the round trip gain $\beta = 3.8$ and the phase bias $\phi_0 = \pi/4$ such that a single uncoupled node behaves chaotically. The digital filter implemented by the DSP board is a two-pole Butterworth bandpass filter with cutoff frequencies $\omega_H/2\pi = 100$ Hz and $\omega_L/2\pi = 2.5$ kHz and a sampling rate of 24 kSamples/s.

For each set of measurements, the nodes are initialized from noise from the electrical signal into the digital signal processing (DSP) board. Then feedback is turned on without coupling, and the opto-electronic oscillators are allowed to oscillate independently until transients die out. At the end of this period, the coupling to the other nodes is turned on and the voltage reading $x(t)$ of each opto-electronic oscillator is recorded on an oscilloscope.

Figure 3 shows some examples of the dynamics displayed by our network of opto-electronic

oscillators. The upper left time series is a measurement of the four opto-electronic oscillators arranged in the five-link network shown. These dynamics are synchronized and are also the dynamics of an individual uncoupled opto-electronic oscillator, since the effect of the Laplacian coupling vanishes for global synchronization. The lower left time series is a measurement of the four opto-electronic oscillators coupled in the eight-link network shown. In this case, the opto-electronic oscillators do not synchronize even though the coupling is strong ($\epsilon = 0.6$).

3.2 Mathematical Model and Numerical Simulations of the Network

The equations governing the dynamics of our network of opto-electronic oscillators are derived in Ref. [72] and are given by

$$\frac{d\mathbf{X}_i(t)}{dt} = \mathbf{E}\mathbf{X}_i(t) - \beta\mathbf{G} \cos^2(X_i^1(t - \tau) + \phi_0) - \epsilon\beta\mathbf{G} \sum_j L_{ij} \cos^2(X_j^1(t - \tau) + \phi_0) + \xi_i(t) \quad (10)$$

where

$$\mathbf{E} = \begin{bmatrix} -(\omega_L + \omega_H) & -\omega_L \\ \omega_L & 0 \end{bmatrix}, \quad \mathbf{G} = \begin{bmatrix} \omega_L \\ 0 \end{bmatrix}, \quad (11)$$

Here $\mathbf{X}_i = [X_i^1(t), X_i^2(t)]^T$ (corresponding to $D_s = 2$ in Eq. (2)) is the state of the digital filter of node i (with $i, j \in \{1, 2, 3, 4\}$, corresponding to $D_n = 4$). By virtue of the second component of \mathbf{G} being zero, coupling between nodes occurs only between X_i^1 and

$X_j^1(i \neq j)$, where $X_i^1(t)$, the normalized voltage of the electrical input to the intensity modulator and is also the only observed variable (i.e., $X_i^1(t) = x(t)$, corresponding to $D'_s = 1$). The nodes are coupled via the Laplacian connectivity matrix L_{ij} , defined so that $L_{ij} = 1$ if there is a link to the first component of the state vector of node i from the first component of the state vector of node j , $L_{ij} = 0$ if there is no such link, and $L_{ii} = -\sum_{j \neq i} L_{ij}$. The coupling strength is given by ϵ , and \mathbf{E} and \mathbf{G} are matrices that describe the filter. Finally, $\xi_i(t) = [\xi_i^1(t), \xi_i^2(t)]^T$ is a vector corresponding to white noise acting independently at each oscillator, and its components have the property that $\langle \xi_i^\mu[s] \xi_j^\nu[t] \rangle = 2\zeta \delta(s-t) \delta_{ij} \delta_{\mu\nu}$ with ζ denoting the strength of the noise.

Since the coupling is between only the first components of the vectors \mathbf{X}_i , we have dropped the component indices in the Laplacian adjacency matrix in Eq. (10). Comparison with Eq. 1 shows that in our example, $\phi_i = \mathbf{E}\mathbf{X}_i(t) - \beta\mathbf{G} \cos^2(X_i^1(t - \tau) + \phi_0) - \epsilon\beta\mathbf{G} \sum_j L_{ij} \cos^2(X_j^1(t - \tau) + \phi_0) + \xi_i(t)$, where we have dropped the component superscripts. The oscillators are identical, so these functions are independent of i , except for the noise term. The relevant partial derivative controlling the propagation of perturbation is $\partial\phi_i^\mu/\partial X_j^\nu \propto L_{ij} \delta_{\mu 1} \delta_{\nu 1}$, for $i \neq j$.

While Eq. (10) accurately describes the behavior of our network of opto-electronic oscillators, numerical simulations are inherently discrete in time. Instead of discretizing Eq. (10) directly, our simulations use a discrete-time model based on the discrete-time filter equations implemented on the DSP board, which can be found in Ref. [74] and is explained in Appendix B. In particular, for this case, we characterize the noise strength by the variable κ , so that $\kappa = \zeta \Delta t$. For the discrete equation that we simulate, the time

step is 0.04ms, which corresponds to the 2.4×10^4 samples/second sampling rate used by the digital filter in our experiment.

Our model is verified by comparison with the experiment, as shown in Fig. 3 for two sets of examples. The top panels of Fig. 3 show measured and simulated time series when all four opto-electronic oscillators are synchronized, and the bottom panels show time series in which none of the oscillators appear to be synchronized.

As we shall see, the degree of synchronization of the oscillators in the network is an important factor in the success of our method to infer the network topology. In order to quantify the degree of global synchrony, we define synchronization error as

$$\text{Synchronization Error} = \frac{1}{D_n(D_n - 1)} \left\langle \sum_{i,j} |x_i(t) - x_j(t)| \right\rangle_t \quad (12)$$

where $\langle \rangle_t$ means time average over a sufficiently long time. This non-negative measure decreases with the amount of synchronization in the system and is zero for perfect global synchrony. For example, in Fig. 3, the synchronized examples (upper panel) have synchronization error ≈ 0.07 , whereas the desynchronized examples (lower panel) have synchronization error ≈ 1.04 .

Using computer simulations, we have studied the dependence of the synchronization error on the network coupling strength ϵ and the number L of network links for all possible directed and connected networks with 4 opto-electronic oscillator nodes. The list of the 62 possible networks is shown in Fig. 4, and is adapted from Ref. [64]. Figure 5 shows the synchronization behavior of these networks as a function of the coupling strength

ϵ for fixed $\beta = 3.8$ and $\phi_0 = \pi/4$. In Fig. 4b, the color coded synchronization error for each of the 62 networks in Fig. 4 is shown as one of the 62 horizontal bars for each value of the coupling strength. Here, the convention we follow is that, for fixed number of links (L), moving upwards, the horizontal bars correspond to the networks listed in Fig. 4 left to right. The same convention is followed in Figs. 6 and 7. The results in Fig. 5 were obtained from numerical simulations without noise ($\kappa = 0$). We see that for intermediate coupling strengths, the networks synchronize, but for small and large coupling strengths, the networks do not synchronize. The seemingly counterintuitive behavior that large coupling strengths lead to desynchronization has been studied for our network of opto-electronic oscillators [75] and is characteristic of delay coupled systems in general [76]. Furthermore, for coupling strengths in the range $\epsilon > 0.5$, for a fixed value of coupling strength, sparser networks are seen to synchronize more readily than densely connected networks. This behavior is also studied and explained in earlier works [75, 77].

4 Results of Link Inference Tests

4.1 Performance on Simulated Data

In this section, we test our methodology on simulated time series data for our coupled opto-electronic oscillator network. We will use these simulation tests to study the effects of noise and coupling strength on the amount of synchrony in the system, and their effect on the performance of link inference tasks. In particular, in the last section (Sec. 3.2)

we showed that our opto-electronic oscillator networks show synchronized dynamics for certain ranges of the coupling strength ϵ . As we will subsequently show, our method works excellently when the system dynamics does not show pronounced global synchrony, while it does not work well when there is pronounced global synchrony. Furthermore, we will show that our technique gives excellent results when there is a small amount of dynamical noise present so that the global synchrony among the opto-electronic oscillators is appreciably broken.

In order to directly demonstrate the effect of loss of synchrony on link inference, we vary the noise level and coupling strength in the following two sets of examples. In the first example set, the system starts with a random initial condition with no noise for 5×10^4 time steps (about 1470 delay times) and is allowed to settle down to an attractor. Then we continue the simulation, but with the noise strength κ set to 10^{-6} for the next 5×10^4 steps, then with the noise strength set to $\kappa = 10^{-4}$ for the next 5×10^4 steps, and so on, keeping the coupling strength fixed at $\epsilon = 0.6$ (Figs. 6(a) and 6(b)). As shown in Fig. 6(b), as the noise strength increases, it drives the system away from the attractor and disrupts its global synchrony, resulting in larger synchronization error, which allows better link inference performance, as shown in Fig. 6(a). In these figures, for each of the time series segments with a fixed noise strength, we use the first 3×10^4 time steps (about 880 delay times) to train our RC and infer links using our procedure described in Sec. 2. We repeat this process for each of the 62 possible connected networks of 4 opto-electronic oscillators [64], each one with a different random initial condition. We use the same procedure in the next set of examples (Figs. 7(a) and 7(b)), but this time

we keep the noise level fixed at its nominal experimental value of $\kappa = 10^{-6}$ and vary the coupling strength ϵ stepwise. The results are summarized in Fig. 7. For both Figs. 6 and 7, we simultaneously plot the number of false positives and synchronization error and follow the same convention as in Fig. 5.

As we see from Fig. 6, regions with a greater degree of global synchronization generally have large false positives errors, consistent with the hypothesis that global synchrony is detrimental to the performance of link inference. This is expected because exact synchronization makes the time series from the 4 opto-electronic oscillators indistinguishable and hence the observed dynamics yields no information about their underlying causal interactions. In particular, we see that networks with 8 or more links do not synchronize sufficiently even in absence of the noise, and we are indeed able to infer the links well, with, at most, only 1 false positive. In contrast, for networks with smaller numbers of links, which are strongly synchronized for noise levels $\kappa \lesssim 10^{-3}$, we have many false positive link inferences. Again, as we see from Fig. 6, all the networks show a loss of global synchrony for sufficiently strong noise levels ($\kappa \gtrsim 10^{-2}$) and this results in almost perfect link inference until the noise strength becomes significant compared to the noiseless opto-electronic oscillator signal amplitudes ($\kappa \gtrsim 10^0$). Other examples of similar beneficial roles of noise in link inference can be found at earlier works as well, e.g., in [25, 29, 78–82].

In the second set of examples (Figs. 7(a) and 7(b)), we fix the noise at a particular strength $\kappa = 10^{-6}$, and progressively increase the coupling strength ϵ . We estimate that this noise level approximates that for the experimental tests reported in the next

subsection (Sec. 4.2). As in the previous examples, Fig. 7 shows that our link inference method performs well when the global synchrony is not too strong. A difference in this set of results from the previous ones is the non-trivial relationship between the coupling strength ϵ and global synchrony, which we have already discussed in the last section (Fig. 5). Furthermore, we notice that, even in the absence of global synchrony, the coupling strength needs to exceed a minimum value (about 0.1) for successful link inference. For smaller coupling, the off-diagonal elements of the matrix $\mathbf{M}[n\Delta t]$ could be so small in magnitude that the values corresponding to actual links are of the same order as those corresponding to absent links. Thus, sufficiently large coupling strength ϵ is beneficial for our link inference technique because of the better contrast among the elements of $\mathbf{M}[n\Delta t]$ and diminished global synchrony.

4.2 Performance on Experimental Data

Having established the usefulness of our network inference method on simulated time series data, we now report our experimental tests on the opto-electronic oscillator networks described in Sec. 4.1. In Fig. 8, we show some representative examples of the performance of our method on experimental time series data. Each column in the figure corresponds to a time-series from a distinct network indicated above the column, with the respective global synchronization error indicated on the horizontal axis. The height of the columns gives the total number of links in the corresponding network. The columns are each divided into three parts (colored in red, green, and black in the plot). The height of the red portion indicates the number of falsely inferred links (“false positives”, FP).

This portion is absent in the many cases where we have perfect network inference. The number of correctly inferred links (“true positives”, TP) is indicated by the total height of the green plus black portions of a column. The height of the black portion indicates the expected number of true positives on average (to nearest integer) that would be obtained if all L links were to be guessed randomly, while the height of the green portion indicates the increase of true positives over what would result from random selection. To evaluate the expected number of randomly selected true positives, we note that, for L links randomly and uniformly assigned among the $D_n(D_n - 1)$ ordered pairs of D_n nodes, the expected number of false positive links is $L \left(1 - \frac{L}{D_n(D_n-1)}\right)$ and the expected number of true positive links is thus $L^2/D_n(D_n - 1)$. If our method yields more true positives than $L^2/D_n(D_n - 1)$, then we consider our method to be successful, even if it gives some false positives.

To summarize our experimental results, consistent with the simulation results of Figs. 5 and 7, the time-series from the experimental opto-electronic oscillator networks (Fig. 8) were either globally well synchronized or else were strongly desynchronized, and, when strong desynchronization applied, our method correctly identified all of the links.

5 Discussion

In this work, we developed a reservoir-computer-based technique for the general problem of link inference of noisy delay-coupled networks from their nodal time series data and demonstrated the success of our method on simulated and experimental data from

opto-electronic oscillator networks. Our main findings are as follows:

- Testing on experimental and simulated time-series datasets from networks, we found that, in the absence of dynamical noise, our method yields extremely good results, as long as there is no synchrony in the system.
- We found that dynamical noise can greatly enhance the performance of our method when synchrony is present provided that the noise amplitude is large enough to perturb the synchrony.
- Since dynamical noise is ubiquitous in natural and experimental situations, we anticipate that, depending on the strength of the noise, this technique may be useful in network inference tasks relevant to fields like biochemistry, neuroscience, ecology, and economics.

Among the important issues for future investigation, our work in this paper could be extended to cases when the dynamics of the network nodal states are partially synchronized (e.g., cluster synchronization of nodes [83]) or display generalized synchronization [84–87]. Effects of network symmetries [83, 88], non-uniform coupling [89], and non-identical oscillators [90] and delay times —all of which can affect the synchrony of nodal states —would also be very interesting to study. Another important issue that awaits study is the effects of incomplete [91], or erroneous nodal state data [92, 93] on link inference.

6 Acknowledgements

This work was supported by the U. S. National Science Foundation Grant DMS 1813027 (AB and EO) and the Office of Naval Research Grant N000142012139 (RR). AB acknowledges that he did this work at the University of Maryland and its neighborhoods in College Park, which stand on the ancestral lands of the Nacotchtank (Anacostan) and Piscataway People.

Appendices

A Determination of the time-delay from cross-correlation

In this Appendix, we demonstrate that the duration of the delay along a link in our network can be accurately estimated from the cross-correlation between the measured time series of the two nodes connected by that link. In particular, we show that the location of the peak of the cross-correlation between the two nodes provides a good estimate of the delay time. We also show that the cross-correlation cannot determine causality, because it cannot determine the direction of a given putative link, or if the link even exists at all.

Consider the network depicted in Fig. 9a, where each node is an opto-electronic oscillator as described in Sec. 3. The delay in each link is $\tau = 1.44\text{ms}$. We define the cross-correlation

between the sampled time series of two nodes i and j as

$$\rho_{ij}(\text{lag}) = \frac{1}{\sigma_i \sigma_j} \sum_k x_i[k + \text{lag}] x_j[k], \quad (\text{A.1})$$

where $x_i[k]$ is the measured time series of node i at discrete time k and σ_i is the RMS value of x_i . The time series should be mean-subtracted so that $\langle x_i \rangle = 0$. The time series used here were obtained from experimental measurements of our opto-electronic oscillator network.

First, we compute ρ_{12} , the cross-correlation between node 1 and node 2, shown in Fig. 9b. A peak is located at -1.44ms. This corresponds to the delay in the link from node 1 to node 2. This suggests that the dynamics of node 2 lag behind the dynamics of node 1, as one might expect since the delayed link is from node 1 to node 2.

Next, we compute ρ_{23} , the cross-correlation between node 2 and node 3, shown in Fig. 9c. The largest (negative, in this case) peak is located at 1.44ms, correctly identifying the absolute value of the delay time of the link from node 2 to node 3. However, in contrast to ρ_{12} , the peak location in ρ_{23} shows that node 3 leads node 2. There is no peak at a lag of -1.44ms. This shows that the cross-correlation can identify the delay time, but not the link direction.

We now consider ρ_{24} . Nodes 2 and 4 have a bidirectional link; however, the cross-correlation ρ_{24} shown in Fig. 9d has a prominent peak at 1.44ms but not at -1.44ms. There is no indication that the link is bidirectional.

Finally, we consider ρ_{14} . There is no direct link between nodes 1 and 4. Still, the

cross-correlation ρ_{24} shown in Fig. 9e has peaks at both 1.44ms but at -1.44ms.

This example demonstrates that the cross-correlation can provide an accurate estimate of the duration of the delay in the coupling between two nodes, but that it does not provide sufficient information to determine the existence or directionality of a link. We find similar results in all the networks of opto-electronic oscillators we tested.

B Derivation of the discrete-time equation for simulating the opto-electronic system

In this appendix, we derive the discrete-time equations implemented by the DSP board in our experimental setup and used in our simulations. These discrete-time equations are derived using standard techniques for approximating an analog filter as a digital filter and are essentially a trapezoid rule approximation to Eqs. 10 and 11.

The derivation here closely follows that presented in Ref. [72]. The missing details from Ref. [72] are filled in here, drawing from Ref. [94] for the details of the z-transform and bilinear transform.

The continuous-time filter equations that describe a two-pole bandpass filter are

$$\frac{d\mathbf{u}(t)}{dt} = \mathbf{E}\mathbf{u}(t) - \mathbf{F}r(t) \tag{B.1}$$

$$x(t) = \mathbf{G}\mathbf{u}(t) \tag{B.2}$$

where

$$\mathbf{E} = \begin{bmatrix} -(\omega_L + \omega_H) & -\omega_L \\ \omega_L & 0 \end{bmatrix}, \quad \mathbf{F} = \begin{bmatrix} \omega_L \\ 0 \end{bmatrix}, \quad \text{and } \mathbf{G} = \begin{bmatrix} 1 & 0 \end{bmatrix}. \quad (\text{B.3})$$

Here, $\mathbf{u}(t)$ is a 2-vector that describes the state of the filter, $r(t)$ is the filter input, and $x(t)$ is the filter output. In the case of one of our opto-electronic oscillators $r(t) = \beta \cos^2(x(t - \tau) + \phi_0)$. In order to implement this filter digitally, one derives the digital filter equations by computing the transfer function of the analog filter, then applying the bilinear transform with frequency pre-warping to the continuous-time transfer function to obtain the discrete-time transfer function. From there, the discrete-time digital filter equations can be written down.

The transfer function $H(s)$ of the analog filter can be found by $H(s) \equiv X(s)/R(s)$, where the capital letters X and R indicate the Laplace transform of x and r , respectively. We compute the Laplace transform of Eq. B.1:

$$s\mathbf{U}(s) = \mathbf{E}\mathbf{U}(s) + \mathbf{F}R(s) \quad (\text{B.4})$$

Then, performing the Laplace transform of Eq. B.2 and inserting Eq. B.4, we have:

$$H(s) \equiv \frac{X(s)}{R(s)} = \mathbf{G}(s\mathbf{I} - \mathbf{E})^{-1}\mathbf{F} = \frac{s\tau_H}{(1 + \tau_L s)(1 + \tau_H s)}, \quad (\text{B.5})$$

where $\tau_H = 1/\omega_H$ and $\tau_L = 1/\omega_L$. Equation B.5 is the continuous time filter transfer function for the filter described by Eqs. B.1-B.3.

Two standard tools used in the design and analysis of digital filters are the z-transform

and the bilinear transform. The z -transform is the discrete time analog of the Laplace transform. The bilinear transform is a tool used to turn a continuous-time filter into a discrete-time filter. It can be shown that the result obtained by the bilinear transform method we use here is equivalent to applying the trapezoidal integration rule to Eqs. B.1-B.3 [94].

The z -transform is defined as

$$Z\{x[n]\} \equiv \sum_{n=-\infty}^{\infty} x[n]z^{-n}, \quad (\text{B.6})$$

where z is a continuous complex variable, and n is discrete time. One important z -transform relations is that a delay by m time steps in the discrete-time domain is equivalent to multiplication by z^{-m} in the z -domain.

The bilinear transform is used to convert our continuous-time filter transfer function (Eq. B.5) into a discrete-time filter transfer function. An exact conversion is done by discretizing with a time-step of T and equating $z = e^{sT}$. Since T is small, we can approximate

$$s = \frac{1}{T} \ln(z) = \frac{2}{T} \frac{1 - z^{-1}}{1 + z^{-1}}. \quad (\text{B.7})$$

Equation B.7 is the bilinear transform. This approximation is equivalent to applying the trapezoid rule to the continuous-time filter equations [94]. When Eq. B.7 is substituted into Eq. B.5, we obtain the transfer function for a discrete-time filter with similar

characteristics to the desired analog filter:

$$H(z) = \frac{1}{4}(1 - z_L)(1 + z_H) \frac{1 - z^{-2}}{(1 - z_L z^{-1})(1 - z_H z^{-1})}. \quad (\text{B.8})$$

This change of variables is a nonlinear mapping, so frequency warping occurs. This effect is minimal when the frequencies are significantly less than the Nyquist frequency (in this case $f_L = 2.5\text{kHz}$ and the Nyquist frequency is 12kHz) and can be further mitigated by pre-warping the frequencies of the continuous-time filter by $\Omega = \frac{2}{T} \tan(\frac{\omega}{2})$, where Ω is the discrete-time frequency and ω is the continuous-time frequency [94]. Therefore, we find that

$$z_H = \frac{1 - \tan(T/2\tau_H)}{1 + \tan(T/2\tau_H)}$$

and

$$z_L = \frac{1 - \tan(T/2\tau_L)}{1 + \tan(T/2\tau_L)}.$$

Now, one can use the definition of the transfer function $H(z) \equiv X(z)/R(z)$ to find

$$(1 - (z_L + z_H)z^{-1} + z_L z_H z^{-2})X(z) = \frac{1}{4}(1 - z_L)(1 + z_H)(1 - z^{-2})R(z). \quad (\text{B.9})$$

We arrive at the discrete-time filter equation by performing the inverse z-transform on Eq. B.9:

$$x[n] = (z_L + z_H)x[n - 1] - z_L z_H x[n - 2] + \frac{1}{4}(1 - z_L)(1 + z_H) (r[n] - r[n - 2]). \quad (\text{B.10})$$

For the filter used in this work, $z_L + z_H = 1.4845$, $z_L z_H = 0.4968$, and $\frac{1}{4}(1 - z_L)(1 + z_H) = 0.242$.

References

- ¹R. Albert and A.-L. Barabasi, “Statistical mechanics of complex networks”, *Rev. Mod. Phys.* **74**, 47 (2002).
- ²J. A. Dunne, R. J. Williams, and N. D. Martinez, “Food-web structure and network theory: the role of connectance and size”, *Proc. Natl. Acad. Sci. USA* **99**, 12917–12922 (2002).
- ³N. D. Price and I. Shmulevich, “Biochemical and statistical network models for systems biology”, *Curr. Opin. Biotech.* **18**, 365–370 (2007).
- ⁴M. Vidal, M. E. Cusick, and A.-L. Barabasi, “Interactome networks and human disease”, *Cell* **144**, 986–998 (2011).
- ⁵A. Baryshnikova, M. Costanzo, C. L. Myers, B. Andrews, and C. Boone, “Genetic interaction networks: toward an understanding of heritability”, *Annu. Rev. Genomics Hum. Genet.* **14**, 111–133 (2013).
- ⁶M. Costanzo, B. VanderSluis, E. N. Koch, A. Baryshnikova, C. Pons, G. Tan, W. Wang, M. Usaj, J. Hanchard, S. D. Lee, et al., “A global genetic interaction network maps a wiring diagram of cellular function”, *Science* **353** (2016).
- ⁷D. S. Bassett and O. Sporns, “Network neuroscience”, *Nat. Neurosci.* **20**, 353–364 (2017).
- ⁸R. Pastor-Satorras, C. Castellano, P. Van Mieghem, and A. Vespignani, “Epidemic processes in complex networks”, *Rev. Mod. Phys.* **87**, 925 (2015).

- ⁹I. M. de Abril, J. Yoshimoto, and K. Doya, “Connectivity inference from neural recording data: challenges, mathematical bases and research directions”, *Neural Netw.* **102**, 120–137 (2018).
- ¹⁰M.-E. Lynall, D. S. Bassett, R. Kerwin, P. J. McKenna, M. Kitzbichler, U. Muller, and E. Bullmore, “Functional connectivity and brain networks in schizophrenia”, *J. Neurosci.* **30**, 9477–9487 (2010).
- ¹¹M. Chavez, M. Valencia, V. Navarro, V. Latora, and J. Martinerie, “Functional modularity of background activities in normal and epileptic brain networks”, *Phys. Rev. Lett.* **104**, 118701 (2010).
- ¹²C. Sima, J. Hua, and S. Jung, “Inference of gene regulatory networks using time-series data: a survey”, *Curr. Genom.* **10**, 416–429 (2009).
- ¹³R. Albert, “Network inference, analysis, and modeling in systems biology”, *The Plant Cell* **19**, 3327–3338 (2007).
- ¹⁴E. L. Sander, J. T. Wootton, and S. Allesina, “Ecological network inference from long-term presence-absence data”, *Sci. Rep.* **7**, 1–12 (2017).
- ¹⁵I. Milns, C. M. Beale, and V. A. Smith, “Revealing ecological networks using bayesian network inference algorithms”, *Ecology* **91**, 1892–1899 (2010).
- ¹⁶J. Runge, V. Petoukhov, J. F. Donges, J. Hlinka, N. Jajcay, M. Vejmelka, D. Hartman, N. Marwan, M. Paluš, and J. Kurths, “Identifying causal gateways and mediators in complex spatio-temporal systems”, *Nat. Commun.* **6**, 1–10 (2015).
- ¹⁷P. Venegas, Tracing the untraceable: AI network inference for the dark web and crypto privacy coins.

- ¹⁸M. Ding, Y. Chen, and S. L. Bressler, Granger causality: basic theory and application to neuroscience, 2006.
- ¹⁹D. Zhou, Y. Xiao, Y. Zhang, Z. Xu, and D. Cai, “Causal and structural connectivity of pulse-coupled nonlinear networks”, *Phys. Rev. Lett.* **111**, 054102 (2013).
- ²⁰T. Schreiber, “Measuring information transfer”, *Phys. Rev. Lett.* **85**, 461 (2000).
- ²¹J. Sun, D. Taylor, and E. M. Bollt, “Causal network inference by optimal causation entropy”, *SIAM J. on Appl. Dyn. Syst.* **14**, 73–106 (2015).
- ²²J. Casadiego, D. Maoutsa, and M. Timme, “Inferring network connectivity from event timing patterns”, *Phys. Rev. Lett.* **121**, 054101 (2018).
- ²³C. Zou and J. Feng, “Granger causality vs. dynamic bayesian network inference: a comparative study”, *BMC Bioinform.* **10**, 1–17 (2009).
- ²⁴T. P. Peixoto, “Network reconstruction and community detection from dynamics”, *Phys. Rev. Lett.* **123**, 128301 (2019).
- ²⁵J. Ren, W.-X. Wang, B. Li, and Y.-C. Lai, “Noise bridges dynamical correlation and topology in coupled oscillator networks”, *Phys. Rev. Lett.* **104**, 058701 (2010).
- ²⁶D. Dahmen, H. Bos, and M. Helias, “Correlated fluctuations in strongly coupled binary networks beyond equilibrium”, *Phys. Rev. X* **6**, 031024 (2016).
- ²⁷S. Leng, Z. Xu, and H. Ma, “Reconstructing directional causal networks with random forest: causality meeting machine learning”, *Chaos* **29**, 093130 (2019).
- ²⁸M. G. Leguia, Z. Levnajic, L. Todorovski, and B. Ženko, “Reconstructing dynamical networks via feature ranking”, *Chaos* **29**, 093107 (2019).

- ²⁹A. Banerjee, J. Pathak, R. Roy, J. G. Restrepo, and E. Ott, “Using machine learning to assess short term causal dependence and infer network links”, *Chaos* **29**, 121104 (2019).
- ³⁰J. Chen, X. Lin, C. Jia, Y. Li, Y. Wu, H. Zheng, and Y. Liu, “Generative dynamic link prediction”, *Chaos* **29**, 123111 (2019).
- ³¹R.-M. Cao, S.-Y. Liu, and X.-K. Xu, “Network embedding for link prediction: the pitfall and improvement”, *Chaos* **29**, 103102 (2019).
- ³²N. Frolov, V. Maksimenko, A. Lüttjohann, A. Koronovskii, and A. Hramov, “Feed-forward artificial neural network provides data-driven inference of functional connectivity”, *Chaos* **29**, 091101 (2019).
- ³³I. Goodfellow, Y. Bengio, A. Courville, and Y. Bengio, Deep learning, Vol. 1 (MIT press Cambridge, 2016).
- ³⁴G. Carleo, I. Cirac, K. Cranmer, L. Daudet, M. Schuld, N. Tishby, L. Vogt-Maranto, and L. Zdeborova, “Machine learning and the physical sciences”, *Reviews of Modern Physics* **91**, 045002 (2019).
- ³⁵G. Tanaka, T. Yamane, J. B. Heroux, R. Nakane, N. Kanazawa, S. Takeda, H. Numata, D. Nakano, and A. Hirose, “Recent advances in physical reservoir computing: a review”, *Neural Netw.* **115**, 100–123 (2019).
- ³⁶J. Pathak, B. Hunt, M. Girvan, Z. Lu, and E. Ott, “Model-free prediction of large spatiotemporally chaotic systems from data: a reservoir computing approach”, *Phys. Rev. Lett.* **120**, 024102 (2018).

- ³⁷J. Pathak, A. Wikner, R. Fussell, S. Chandra, B. R. Hunt, M. Girvan, and E. Ott, “Hybrid forecasting of chaotic processes: using machine learning in conjunction with a knowledge-based model”, *Chaos* **28**, 041101 (2018).
- ³⁸G. Neofotistos, M. Mattheakis, G. D. Barmparis, J. Hizanidis, G. P. Tsironis, and E. Kaxiras, “Machine learning with observers predicts complex spatiotemporal behavior”, *Front. Phys.* **7**, 24 (2019).
- ³⁹R. S. Zimmermann and U. Parlitz, “Observing spatio-temporal dynamics of excitable media using reservoir computing”, *Chaos* **28**, 043118 (2018).
- ⁴⁰J. Pathak, Z. Lu, B. R. Hunt, M. Girvan, and E. Ott, “Using machine learning to replicate chaotic attractors and calculate lyapunov exponents from data”, *Chaos* **27**, 121102 (2017).
- ⁴¹S. Krishnagopal, M. Girvan, E. Ott, and B. R. Hunt, “Separation of chaotic signals by reservoir computing”, *Chaos* **30**, 023123 (2020).
- ⁴²Z. Lu, J. Z. Kim, and D. S. Bassett, “Supervised chaotic source separation by a tank of water”, *Chaos* **30**, 021101 (2020).
- ⁴³Y. K. Chembo, “Machine learning based on reservoir computing with time-delayed optoelectronic and photonic systems”, *Chaos* **30**, 013111 (2020).
- ⁴⁴D. Markovic, A. Mizrahi, D. Querlioz, and J. Grollier, “Physics for neuromorphic computing”, arXiv preprint arXiv:2003.04711 (2020).

- ⁴⁵L. Larger, A. Baylon-Fuentes, R. Martinenghi, V. S. Udaltsov, Y. K. Chembo, and M. Jacquot, “High-speed photonic reservoir computing using a time-delay-based architecture: million words per second classification”, *Phys. Rev. X* **7**, 011015 (2017).
- ⁴⁶Q. Vinckier, F. Duport, A. Smerieri, K. Vandoorne, P. Bienstman, M. Haelterman, and S. Massar, “High-performance photonic reservoir computer based on a coherently driven passive cavity”, *Optica* **2**, 438–446 (2015).
- ⁴⁷F. Duport, A. Smerieri, A. Akrout, M. Haelterman, and S. Massar, “Fully analogue photonic reservoir computer”, *Sci. Rep.* **6**, 22381 (2016).
- ⁴⁸B. Schrauwen, M. D’Haene, D. Verstraeten, and J. Van Campenhout, “Compact hardware liquid state machines on FPGA for real-time speech recognition”, *Neural Netw.* **21**, 511–523 (2008).
- ⁴⁹L. Appeltant, M. C. Soriano, G. Van der Sande, J. Danckaert, S. Massar, J. Dambre, B. Schrauwen, C. R. Mirasso, and I. Fischer, “Information processing using a single dynamical node as complex system”, *Nat. Commun.* **2**, 1–6 (2011).
- ⁵⁰E. J. Molinelli, A. Korkut, W. Wang, M. L. Miller, N. P. Gauthier, X. Jing, P. Kaushik, Q. He, G. Mills, D. B. Solit, et al., “Perturbation biology: inferring signaling networks in cellular systems”, *PLoS Comput. Biol.* **9**, e1003290 (2013).
- ⁵¹A. Das and I. R. Fiete, “Systematic errors in connectivity inferred from activity in strongly recurrent networks”, *Nat. Neurosci.* **23**, 1286–1296 (2020).
- ⁵²C. Olsen, K. Fleming, N. Prendergast, R. Rubio, F. Emmert-Streib, G. Bontempi, B. Haibe-Kains, and J. Quackenbush, “Inference and validation of predictive gene networks from biomedical literature and gene expression data”, *Genomics* **103**, 329–336 (2014).

- ⁵³X. S. Yao and L. Maleki, “Optoelectronic microwave oscillator”, *J. Opt. Soc. Am. B* **13**, 1725–1735 (1996).
- ⁵⁴Y. C. Kouomou, P. Colet, L. Larger, and N. Gastaud, “Chaotic breathers in delayed electro-optical systems”, *Phys. Rev. Lett.* **95**, 203903 (2005).
- ⁵⁵K. E. Callan, L. Illing, Z. Gao, D. J. Gauthier, and E. Scholl, “Broadband chaos generated by an optoelectronic oscillator”, *Phys. Rev. Lett.* **104**, 113901 (2010).
- ⁵⁶L. Larger, M. C. Soriano, D. Brunner, L. Appeltant, J. M. Gutierrez, L. Pesquera, C. R. Mirasso, and I. Fischer, “Photonic information processing beyond turing: an optoelectronic implementation of reservoir computing”, *Opt. Express* **20**, 3241–3249 (2012).
- ⁵⁷Y. Paquot, F. Duport, A. Smerieri, J. Dambre, B. Schrauwen, M. Haelterman, and S. Massar, “Optoelectronic reservoir computing”, *Sci. Rep.* **2**, 287 (2012).
- ⁵⁸A. Argyris, D. Syvridis, L. Larger, V. Annovazzi-Lodi, P. Colet, I. Fischer, J. Garcia-Ojalvo, C. R. Mirasso, L. Pesquera, and K. A. Shore, “Chaos-based communications at high bit rates using commercial fibre-optic links”, *Nature* **438**, 343–346 (2005).
- ⁵⁹J. Yao, “Optoelectronic oscillators for high speed and high resolution optical sensing”, *Journal of Lightwave Technology* **35**, 3489–3497 (2017).
- ⁶⁰L. Larger and J. M. Dudley, “Optoelectronic chaos”, *Nature* **465**, 41–42 (2010).
- ⁶¹L. Larger, “Complexity in electro-optic delay dynamics: modelling, design and applications”, *Phil. Trans. R. Soc. A* **371**, 20120464 (2013).

- ⁶²Y. K. Chembo, D. Brunner, M. Jacquot, and L. Larger, “Optoelectronic oscillators with time-delayed feedback”, *Rev. Mod. Phys.* **91**, 035006 (2019).
- ⁶³L. Illing, C. D. Panda, and L. Shareshian, “Isochronal chaos synchronization of delay-coupled optoelectronic oscillators”, *Phys. Rev. E* **84**, 016213 (2011).
- ⁶⁴B. Ravoori, A. B. Cohen, J. Sun, A. E. Motter, T. E. Murphy, and R. Roy, “Robustness of optimal synchronization in real networks”, *Phys. Rev. Lett.* **107**, 034102 (2011).
- ⁶⁵C. R. Williams, T. E. Murphy, R. Roy, F. Sorrentino, T. Dahms, and E. Scholl, “Experimental observations of group synchrony in a system of chaotic optoelectronic oscillators”, *Phys. Rev. Lett.* **110**, 064104 (2013).
- ⁶⁶J. D. Hart, K. Bansal, T. E. Murphy, and R. Roy, “Experimental observation of chimera and cluster states in a minimal globally coupled network”, *Chaos* **26**, 094801 (2016).
- ⁶⁷A. E. Hoerl and R. W. Kennard, “Ridge regression: biased estimation for nonorthogonal problems”, *Technometrics* **12**, 55–67 (1970).
- ⁶⁸T. Lymburn, D. M. Walker, M. Small, and T. Jüngling, “The reservoir’s perspective on generalized synchronization”, *Chaos* **29**, 093133 (2019).
- ⁶⁹Z. Lu, B. R. Hunt, and E. Ott, “Attractor reconstruction by machine learning”, *Chaos* **28**, 061104 (2018).
- ⁷⁰E. Bollt, On explaining the surprising success of reservoir computing forecaster of chaos, 2020.

- ⁷¹R. Penrose, “A generalized inverse for matrices”, in Mathematical proceedings of the Cambridge philosophical society, Vol. 51, 3 (Cambridge University Press, 1955), pp. 406–413.
- ⁷²T. E. Murphy, A. B. Cohen, B. Ravoori, K. R. Schmitt, A. V. Setty, F. Sorrentino, C. R. Williams, E. Ott, and R. Roy, “Complex dynamics and synchronization of delayed-feedback nonlinear oscillators”, *Phil. Trans. R. Soc. A* **368**, 343–366 (2010).
- ⁷³J. D. Hart, L. Larger, T. E. Murphy, and R. Roy, “Delayed dynamical systems: networks, chimeras and reservoir computing”, *Philosophical Transactions of the Royal Society A* **377**, 20180123 (2019).
- ⁷⁴J. D. Hart, “Experiments on networks of coupled opto-electronic oscillators and phys. random number generators”, PhD thesis (2018).
- ⁷⁵J. D. Hart, J. P. Pade, T. Pereira, T. E. Murphy, and R. Roy, “Adding connections can hinder network synchronization of time-delayed oscillators”, *Phys. Rev. E* **92**, 022804 (2015).
- ⁷⁶V. Flunkert, S. Yanchuk, T. Dahms, and E. Scholl, “Synchronizing distant nodes: a universal classification of networks”, *Phys. Rev. Lett.* **105**, 254101 (2010).
- ⁷⁷A. Townsend, M. Stillman, and S. H. Strogatz, “Dense networks that do not synchronize and sparse ones that do”, *Chaos* **30**, 083142 (2020).
- ⁷⁸M. J. Panaggio, M.-V. Ciocanel, L. Lazarus, C. M. Topaz, and B. Xu, “Model reconstruction from temporal data for coupled oscillator networks”, *Chaos* **29**, 103116 (2019).

- ⁷⁹M. G. Leguia, C. G. Martinez, I. Malvestio, A. T. Campo, R. Rocamora, Z. Levnajic, and R. G. Andrzejak, “Inferring directed networks using a rank-based connectivity measure”, *Phys. Rev. E* **99**, 012319 (2019).
- ⁸⁰J. Lipinski-Kruszka, J. Stewart-Ornstein, M. W. Chevalier, and H. El-Samad, “Using dynamic noise propagation to infer causal regulatory relationships in biochemical networks”, *ACS Synth. Biol.* **4**, 258–264 (2015).
- ⁸¹R. J. Prill, R. Vogel, G. A. Cecchi, G. Altan-Bonnet, and G. Stolovitzky, “Noise-driven causal inference in biomolecular networks”, *PloS One* **10**, e0125777 (2015).
- ⁸²W.-X. Wang, J. Ren, Y.-C. Lai, and B. Li, “Reverse engineering of complex dynamical networks in the presence of time-delayed interactions based on noisy time series”, *Chaos* **22**, 033131 (2012).
- ⁸³L. M. Pecora, F. Sorrentino, A. M. Hagerstrom, T. E. Murphy, and R. Roy, “Cluster synchronization and isolated desynchronization in complex networks with symmetries”, *Nat. Commun.* **5**, 1–8 (2014).
- ⁸⁴N. F. Rulkov, M. M. Sushchik, L. S. Tsimring, and H. D. Abarbanel, “Generalized synchronization of chaos in directionally coupled chaotic systems”, *Phys. Rev. E* **51**, 980 (1995).
- ⁸⁵L. Kocarev and U. Parlitz, “Generalized synchronization, predictability, and equivalence of unidirectionally coupled dynamical systems”, *Phys. Rev. Lett.* **76**, 1816 (1996).
- ⁸⁶D. Senthilkumar, M. Lakshmanan, and J. Kurths, “Transition from phase to generalized synchronization in time-delay systems”, *Chaos* **18**, 023118 (2008).

- ⁸⁷D. Senthilkumar, R. Suresh, M. Lakshmanan, and J. Kurths, “Global generalized synchronization in networks of different time-delay systems”, *Europhys. Lett.* **103**, 50010 (2013).
- ⁸⁸A. J. Whalen, S. N. Brennan, T. D. Sauer, and S. J. Schiff, “Observability and controllability of nonlinear networks: the role of symmetry”, *Phys. Rev. X* **5**, 011005 (2015).
- ⁸⁹M. Denker, M. Timme, M. Diesmann, F. Wolf, and T. Geisel, “Breaking synchrony by heterogeneity in complex networks”, *Phys. Rev. Lett.* **92**, 074103 (2004).
- ⁹⁰T. Nishikawa, A. E. Motter, Y.-C. Lai, and F. C. Hoppensteadt, “Heterogeneity in oscillator networks: are smaller worlds easier to synchronize?”, *Phys. Rev. Lett.* **91**, 014101 (2003).
- ⁹¹X. Han, Z. Shen, W.-X. Wang, and Z. Di, “Robust reconstruction of complex networks from sparse data”, *Phys. Rev. Lett.* **114**, 028701 (2015).
- ⁹²T. P. Peixoto, “Reconstructing networks with unknown and heterogeneous errors”, *Phys. Rev. X* **8**, 041011 (2018).
- ⁹³D. Napoletani and T. D. Sauer, “Reconstructing the topology of sparsely connected dynamical networks”, *Phys. Rev. E* **77**, 026103 (2008).
- ⁹⁴A. V. Oppenheim, J. R. Buck, and R. W. Schaffer, Discrete-time signal processing. vol. 2 (Upper Saddle River, NJ: Prentice Hall, 2001).

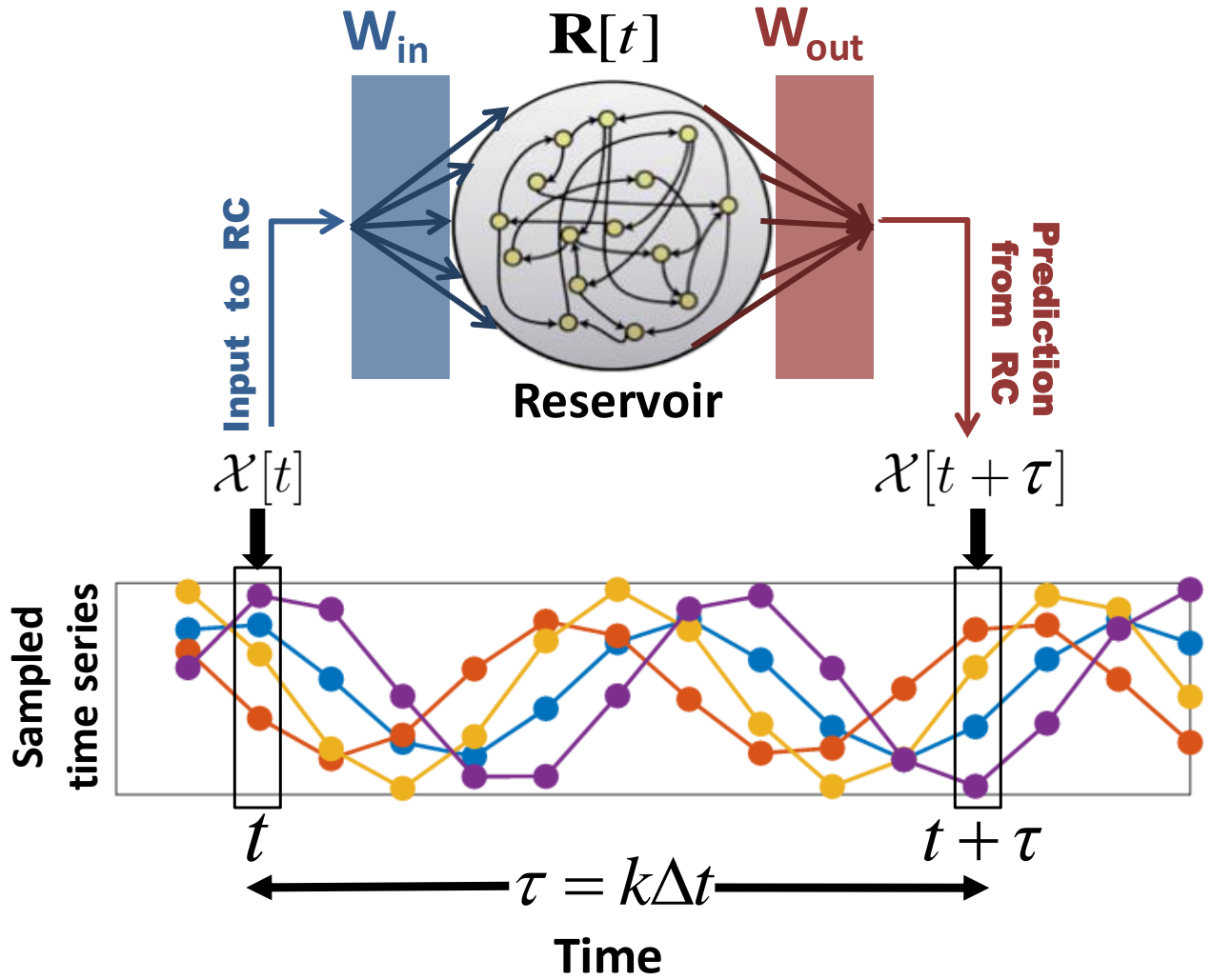


Figure 1: Schematics of the reservoir computer (RC) trained for predicting the time series k time steps ahead

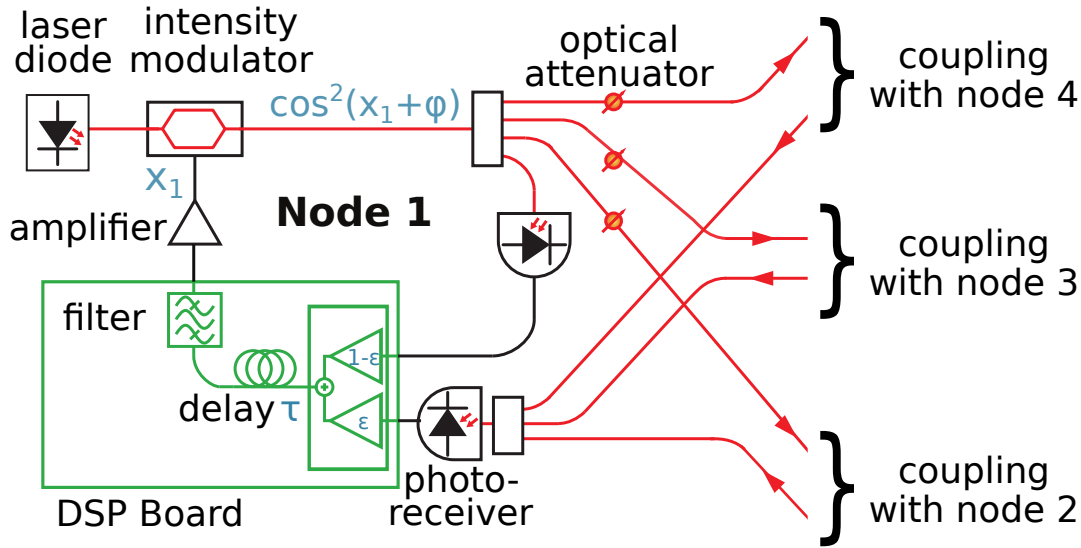


Figure 2: Illustration of opto-electronic oscillator and coupling scheme. Red lines indicate signal paths in optical fibers. Black lines are used to indicate electronic signals, and green indicates the digital signal processing (DSP) board.

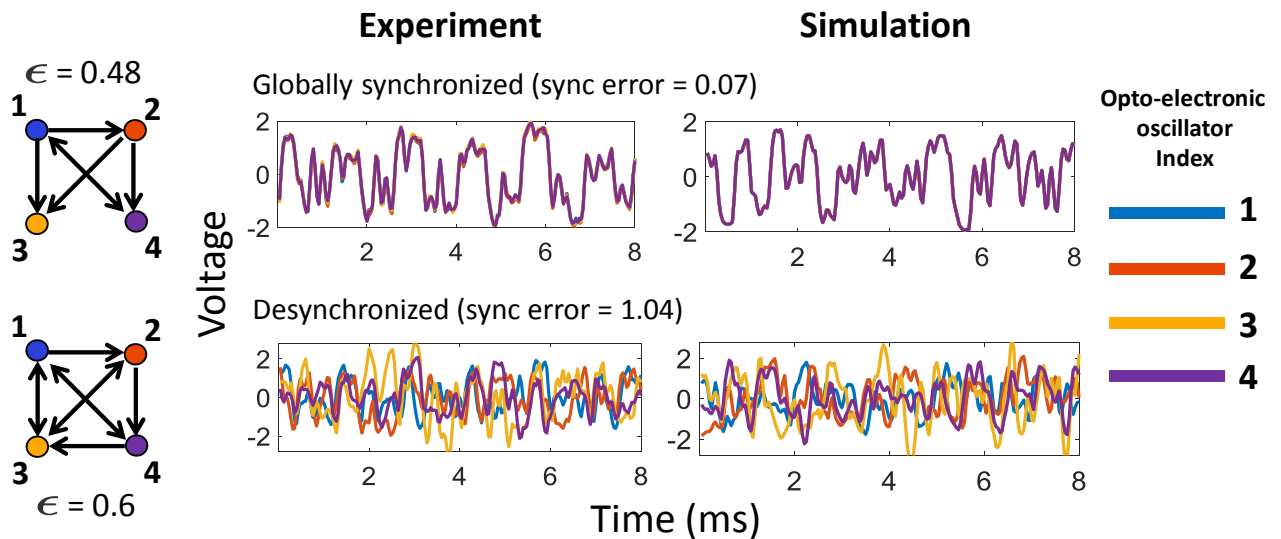


Figure 3: Examples of experimental and simulated time series from two opto-electronic oscillator networks showing globally synchronous (upper panels) and completely desynchronized (lower panels) behavior respectively. For the simulations, we have used the noise strength $\kappa = 10^{-6}$.

L	Possible connected network topologies
12	
11	
10	
9	
8	
7	
6	
5	
4	
3	

Figure 4: List of possible connected directed 4-node networks [64] with different numbers of links (L).

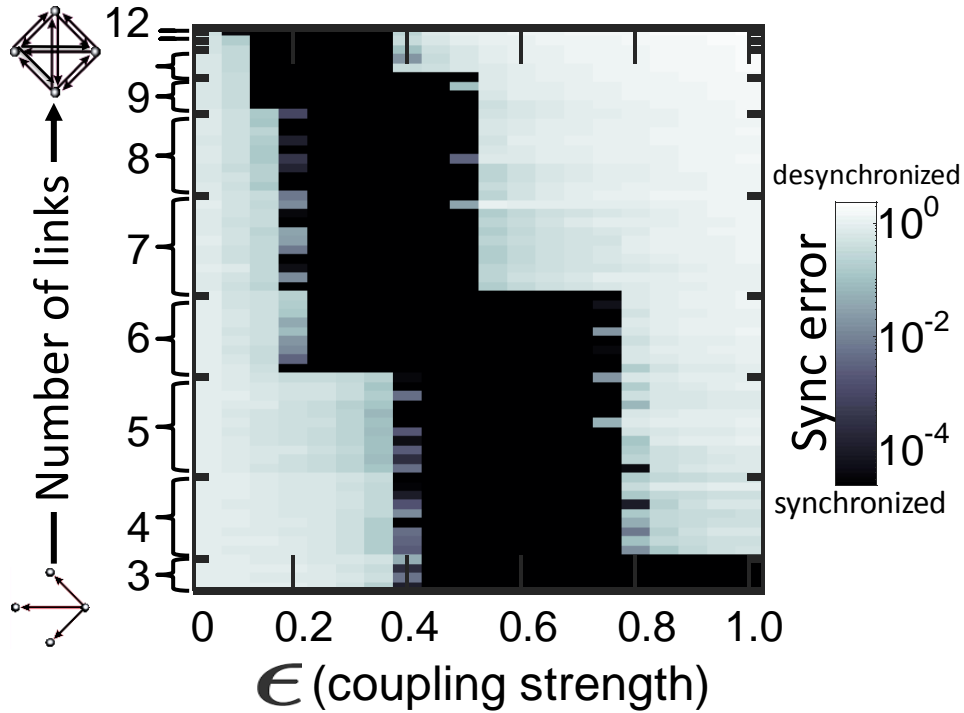
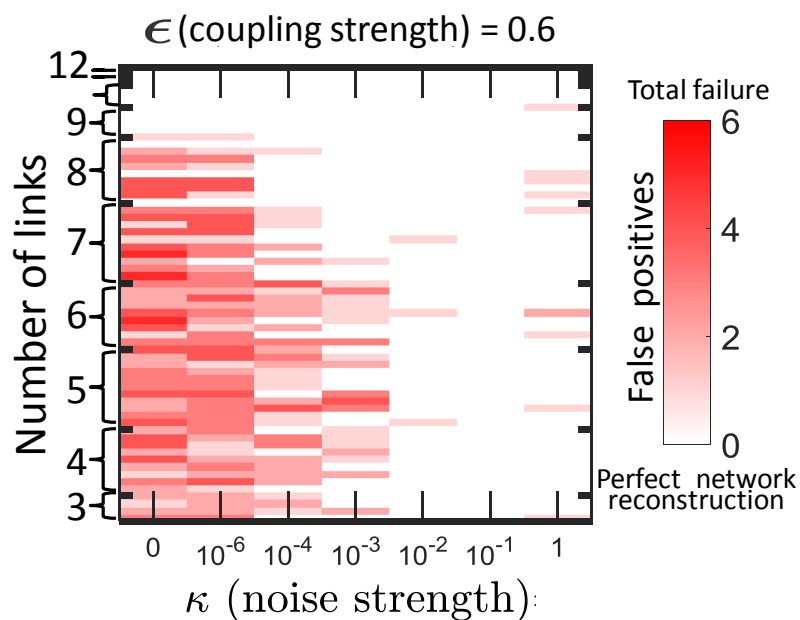


Figure 5: Synchronization error for simulated time series of these networks realized with opto-electronic oscillator nodes with different coupling strengths for random initial conditions. The color coded synchronization error for each of the 62 networks in Fig. 4 is shown as one of the 62 horizontal bars for each value of the coupling strength. Here, the convention we follow is that, for fixed number of links (L), moving upwards, the horizontal bars correspond to the networks listed in Fig. 4 left to right. The same convention is followed in Figs. 6 and 7.

(a)



(b)

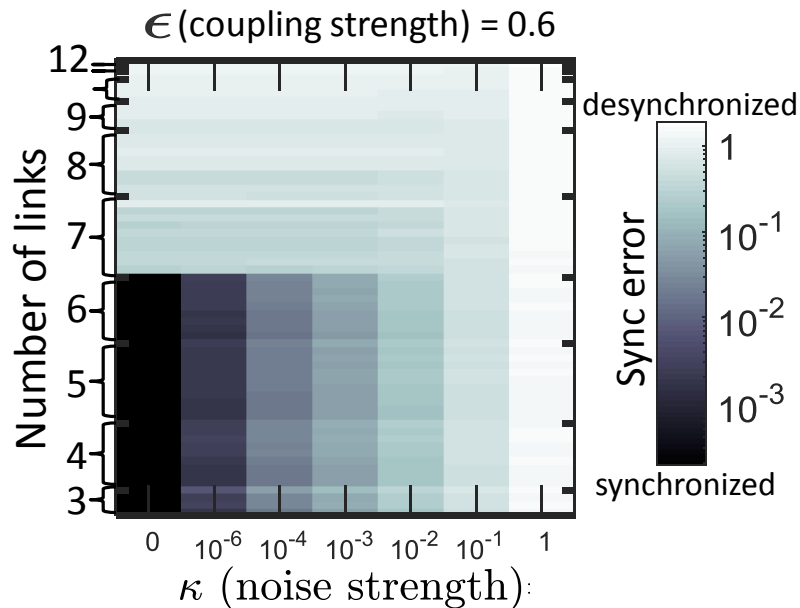
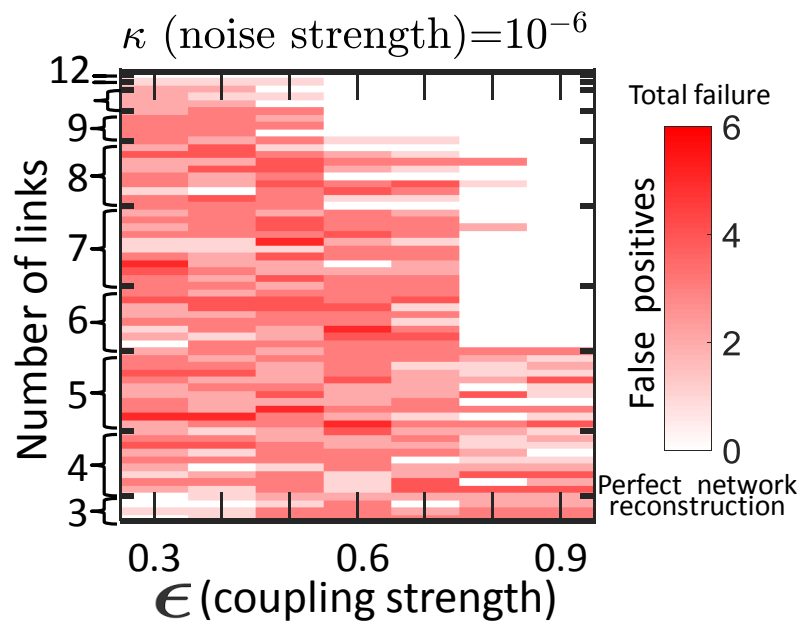


Figure 6: (a) Number of false positives and (b) synchronization error for simulated time series from different networks with progressively increasing noise. Each horizontal cut of the plots represents a single trajectory of the system, starting from a random initial condition. The convention for sequence of the networks is the same as in Fig. 5.

(a)



(b)

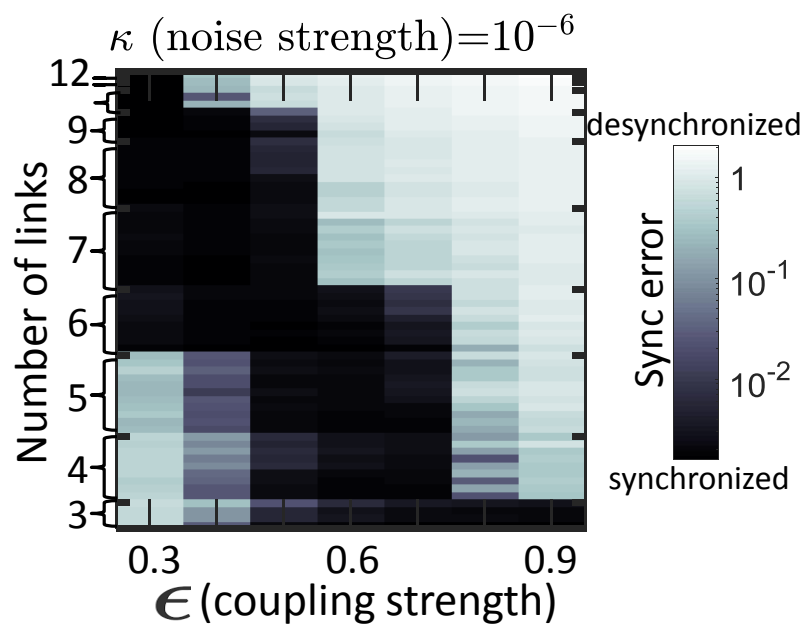


Figure 7: (a) Number of false positives and (b) synchronization error for simulated time series from different networks with progressively increasing coupling strength. Each horizontal cut of the plots represents a single trajectory of the system, starting from a random initial condition. The convention for sequence of the networks is the same as in Fig. 5.

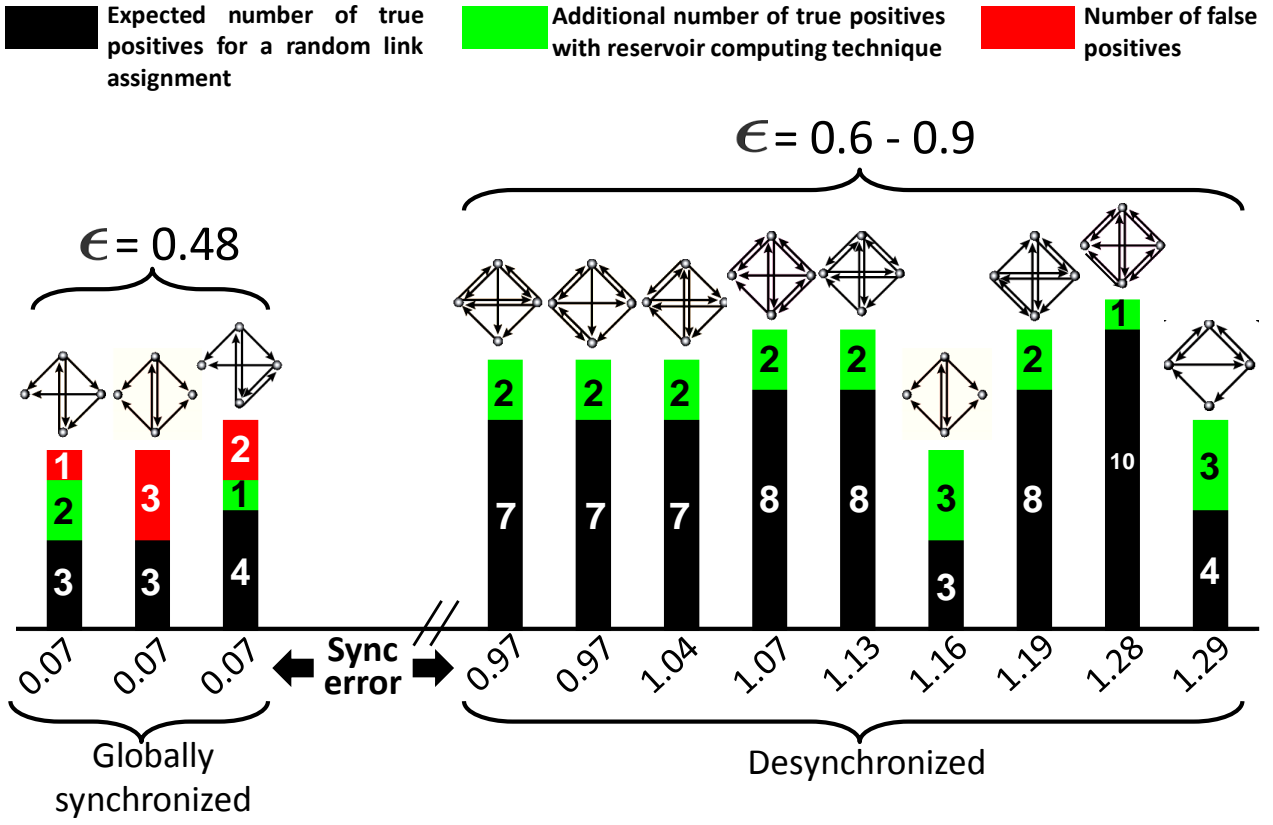


Figure 8: Performance of our network inference method on experimental data. Each of the bars correspond to the experimental realization of a distinct opto-electronic oscillator network, with the height indicating the corresponding number of links. Each bar is separated into 3 segments as shown, but in many of them only two are seen if there is a perfect link inference. The numbers inside the segments indicate the corresponding heights of the segments, rounded to the nearest integers. Ranges of coupling strength (ϵ) and synchronization error for all the examples are indicated as well

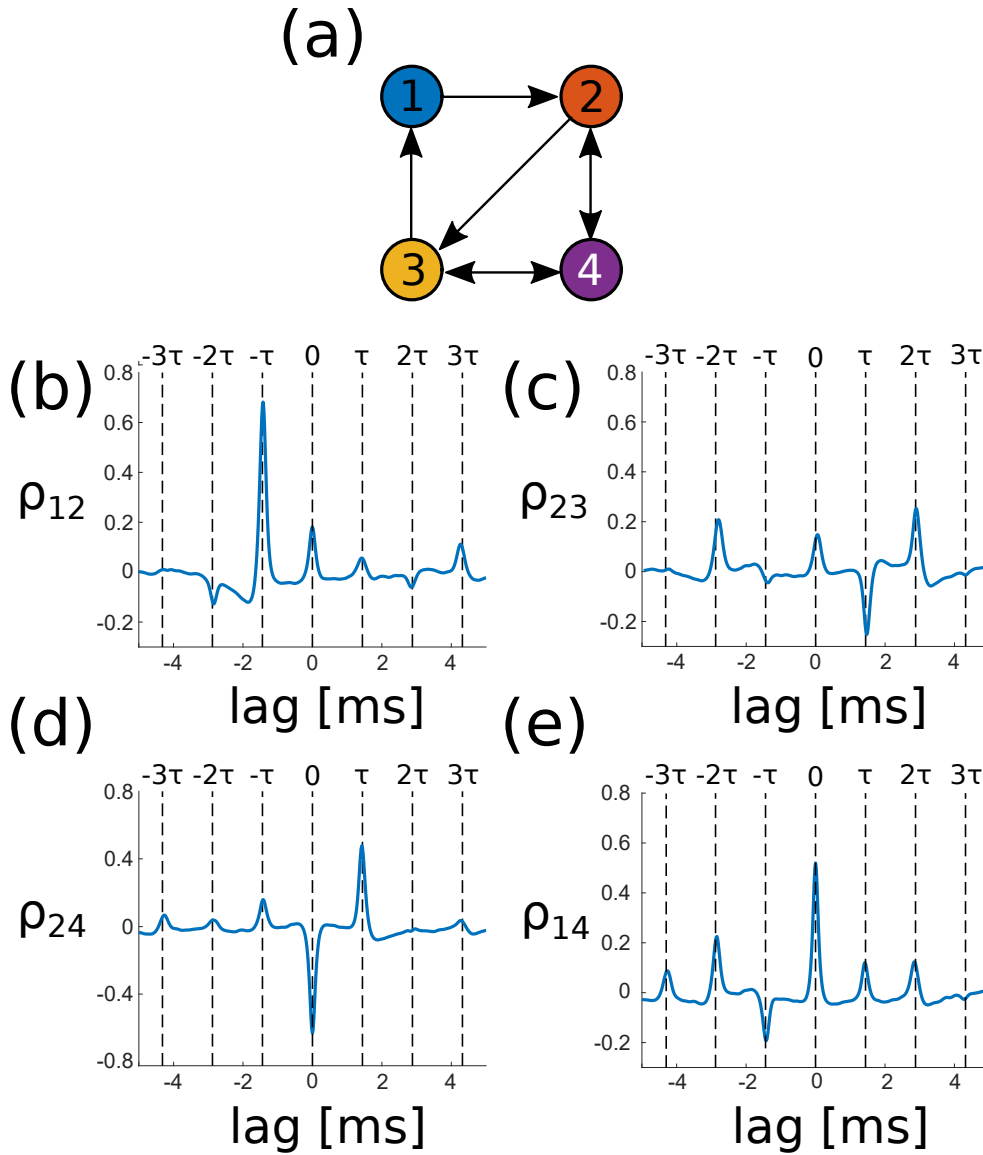


Figure 9: Time delay determination by cross-correlation of measured time series. In all cases, the coupling delay time is 1.44ms. (a) The network to be inferred from time series measurements. (b) The cross-correlation between the time series of nodes 1 and 2. A strong peak is observed near -1.44ms. (c) The cross-correlation between the time series of nodes 2 and 3. A strong negative peak is observed near 1.44ms and a strong positive peak near -1.44ms. (d) The cross-correlation between the time series of nodes 2 and 4. A strong peak is observed near 1.44ms. (e) The cross-correlation between the time series of nodes 1 and 4. Peaks are observed at 1.44ms and -1.44ms, even though there is no link from node 1 to node 4.